The effects of absorption and inelastic scattering of high-resolution electron microscopic images of $YBa_2Cu_3O_{7-x}$

1989 J. Phys.: Condens. Matter 1 1561

(http://iopscience.iop.org/0953-8984/1/9/002)

J. Phys.: Condens. Matter 1 (1989) 1561–1570. Printed in the UK

The effects of absorption and inelastic scattering of high-resolution electron microscopic images of $YBa_2Cu_3O_{7-x}$

D Tang†, R D Brydson†, D A Jefferson† and J M Thomas‡

† Department of Physical Chemistry, University of Cambridge, Lensfield Road, Cambridge CB2 1EP, UK

‡ Davy–Faraday Research Laboratory, The Royal Institution of Great Britain, 21 Albemarle Street, London W1X 4BS, UK

Received 26 August 1988

Abstract. The computational procedures necessary to include the effects of physical absorption and the elastic scattering of initially inelastically scattered electrons in a computer-simulated high-resolution electron microscopic image are outlined. Results of a study of this type carried out on the high-T_c superconductor $YBa_2Cu_3O_{7-x}$ are described, using the plasmon-loss data derived from experimental electron energy-loss spectra, initially by taking the two effects separately but also by considering them together, and an assessment of the approximations used is made. The results indicate that, for a specimen thickness of 8 nm, both processes have only a slight effect on the image contrast, but the influence of absorption is the more significant.

1. Introduction

High-resolution electron microscopy (HREM) has now become an accepted method of determining the cation positions in complex or disordered structures, particularly in oxide phases (see, for example, Iijima and Allpress 1974, Ekstrom and Tilley 1978, Grzinic *et al* 1983) where the inter-cation distances are well within the resolution limits (Cowley 1979) of modern electron microscopes. More recently, in addition to the elucidation of the basic arrangement, some degree of structural refinement has proved possible (Jefferson *et al* 1984), and the method can also be applied to structures where the unit cell lacks the short axis of projection necessary for earlier studies (Zhou *et al* 1986), although in such cases a semi-intuitive image interpretation, normally necessary for the construction of an initial model structure, is no longer possible. To date, most methods of HREM image interpretation have been uniformly based on the principle that the specimen acts as a purely *phase* object, initially using the weak-phase-object approximation (WPOA), in which all dynamical scattering is neglected (Hanzen 1971), progressing to the projected charge-density model (Allpress *et al* 1972) for thicker or more strongly scattering specimens, and finally, when the scattering can no longer be regarded as emanating from a single plane in the crystal, using the multi-slice algorithm (Cowley and Moodie 1957, Goodman and Moodie 1974) which provides a trial-and-error means of testing and refining a model structure.

0953-8984/89/091561 + 10 $02.50

However, in addition to phase contrast, *amplitude* contrast, arising from the removal of electrons from the elastically scattered image, either by incoherent inelastic loss processes, or by scattering outside the objective aperture, plays an important part in the overall image formation. Until recently, this amplitude scattering has only been considered in images of comparatively thick specimens at relatively moderate resolution (Grinton and Cowley 1971, Crowther and Klug 1975), on the one hand because of the belief that, in the very thin specimens necessary for intuitive HREM image interpretation, inelastic processes are of negligible importance, and also because with most HREM instrumentation the limit of resolution is set by factors such as electrical and mechanical instabilities and beam divergence which make consideration of electron removal by scattering outside the objective aperture unnecessary. In addition, for the case of inelastic processes, the lack of a suitable means to measure interaction cross sections or absorption coefficients, or to obtain some estimate of the specimen thickness if the former are known, has been an important factor in this comparative lack of attention.

Even with the most modern HREM instruments, the limit of resolution is still set by instrumental factors and consideration of the electrons removed from the image by the objective aperture ('diffraction contrast') may be neglected unless a deliberate decision is made to introduce an unusually small aperture. If this is the case, the accepted methods of image analysis and simulation can readily deal with this source of contrast. Electrons lost from the *elastic* image by *inelastic* processes, however, may have a considerable importance, particularly in structures containing heavy atoms, and especially in cases where the positions of relatively light atoms are required in a matrix of much heavier ones. The problem with these inelastic electrons is twofold, namely the effect that they have on the elastic image because of their removal from it, and any subsequent effects that arise from their presence in the final electron wavefront, albeit at slightly lower energies. Removal from the elastic image can be treated relatively easily, simply by introducing an absorption factor for each atom in the structure, usually represented as an imaginary part of the scattering factor, if the relevant data are available, but the subsequent role of the inelastic electrons is more uncertain. In the past, it has generally been assumed that these electrons, produced by incoherent scattering events, will merely go to form a constant background or noise level, which will increase in magnitude with specimen thickness, and will not give rise to any periodic contrast features, but more recent studies on specimens thin enough for HREM imaging (Boothroyd and Stobbs 1987, Stobbs and Saxton 1989) have suggested that this may be an over-simplification, and that it is also necessary to consider subsequent *elastic* scattering of these initially *inelastic* electrons. Such scattering, because it arises from the periodic crystal structure, will inevitably lead to periodic contrast features, and these may alter or obscure the features of the elastic image.

The simplest way to remove these complications is to introduce some form of energy filtering, thereby ensuring that the recorded image results only from elastically scattered electrons, and some attempts have been made in this direction (Hashimoto 1985, Lanio *et al* 1986), but an alternative approach, if the type and extent of the energy-loss processes can be measured, is to use computer simulation procedures to assess the influence of the inelastic electrons on the final image, and to determine the specimen thicknesses at which the effect becomes pronounced. In this paper we present the results of a study of this type on a material where these effects might be expected to be significant, namely the high-T_C superconductor $YBa_2Cu_3O_{7-x}$, where both detailed cation and oxygen positions are of considerable importance.

Table 1. Principal peaks in the deconvoluted EELS of $YBa_2Cu_3O_{7-x}$.

Peak	Energy loss (eV)	FWHM (eV)	Weight	Defocus shift (nm)	Focal spread (nm)
I	0.0	2.7	0.831	0.0	14.2
II	11.5	8.0	0.022	+60.4	44.6
III	25.1	18.0	0.147	+131.8	108.1

2. Experimental and computational details

All the simulated images presented below were calculated with standard multi-slice programs using the electron–optical parameters of the top-entry version of the JEOL JEM-200CX electron microscope, namely $C_s = 1.2$ mm, $C_c = 1.4$ mm, 200 kV, voltage and lens instabilities of 2×10^{-6} and 1×10^{-6} respectively, and an energy spread in the electron beam of 1.5 V, typical of that from a LaB_6 cathode. From the measured width of the divergence disc in the selected-area electron diffraction mode it was ascertained that the factor limiting the ultimate resolution was not beam divergence but chromatic factors: consequently the former was not included in the lattice image simulations and the latter was incorporated using an image-averaging method, the average being made over a maximum of 95 images calculated within the focal spread. Electron energy-loss spectra (EELS) were measured for $YBa_2Cu_3O_{7-x}$ using a Gatan 607 spectrometer fitted to a JEM-200CX and interfaced to a Canberra series 80 multi-channel analyser. The energy resolution was approximately 2 eV which was quite adequate for this study. A full description of the complete low-loss region of the spectrum of $YBa_2Cu_3O_{7-x}$ has been given by Yuan *et al* (1988).

Spectra were deconvoluted to remove multiple inelastic scattering using the Fourier–log method described by Williams *et al* (1985), this producing the spectrum that would be obtained from a very thin specimen (where the dominant process is single inelastic scattering) such as that employed in HREM imaging. Analysis of the weights of the plasmon-loss peaks in this deconvoluted spectrum can then be used to make an estimate of the bulk absorption coefficient of the specimen. Comparison of the relative areas and full-width half-height maxima of the two prominent plasmon-loss peaks in the deconvoluted EELS spectra relative to that of the no-loss peak provided the weights and focal spreads of the inelastic images: these data are given in table 1, and the actual EELS spectrum, which contains only one low-loss peak of complex shape, is shown at the top of figure 1. Elastic and inelastic images were summed, after the appropriate weighting, by the same routine as was used to simulate focal spread.

3. Results and discussion

3.1. Pure absorption

In a multi-slice calculation, if the effects of absorption are to be considered, the transmission function for a single slice becomes

$$q(x, y) = \exp[-i(\sigma - i\gamma)\varphi(x, y)]$$

where γ is the bulk absorption coefficient and σ is given by

$$\sigma = \pi/[\lambda V_0 (1 + eV_0/2m_0c^2)]$$

where λ is the wavelength of the incident electrons, V_0 the accelerating voltage, e the

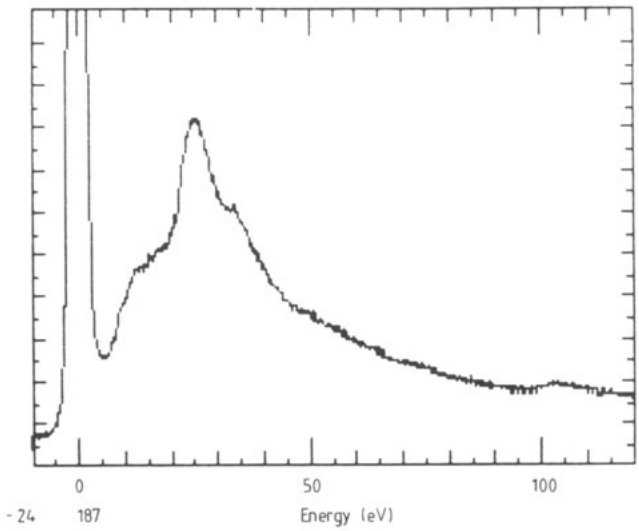

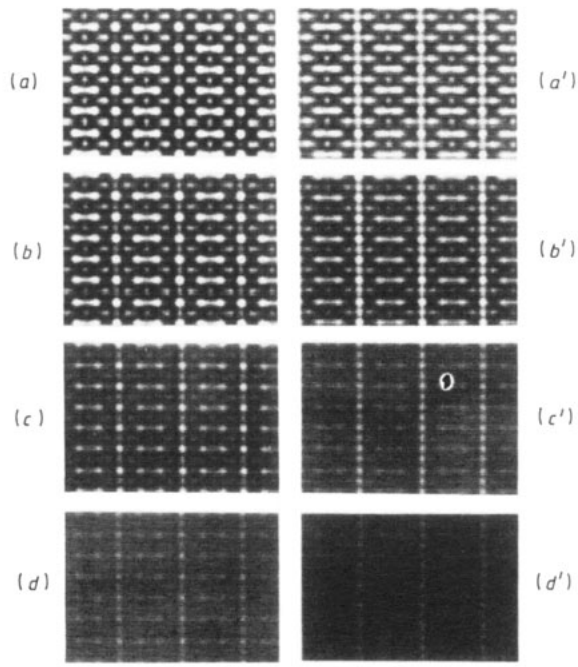

Figure 1. The deconvoluted EELS spectrum of $YBa_2Cu_3O_{7-x}$, with simulated images down [100] ((*a*)–(*d*)) and [010] ((*a'*)–(*d'*)) showing the effect of progressively greater absorption. The values of the absorption coefficient y used are 0.0000 ((*a*), (*a'*)), 0.0001 ((*b*), (*b'*)), 0.0003 ((*c*), (*c'*)) and 0.0005 ((*d*), (*d'*)). The limiting resolution used was set at 0.19 nm, with a specimen thickness of 8.0 nm, and the contrast scale was constant throughout.

electronic charge, m_0 the electron rest mass and c the velocity of light in vacuum. $\varphi(x, y)$ is the total projected potential in a slice of thickness Δz, and generally γ is relatively small with, for the case of $YBa_2Cu_3O_{7-x}$ and $z = 0.2$ nm, the maximum value of $\gamma\varphi(x, y)$

being less than 0.1. The principal difficulty in assessing the effect of absorption in multi-slice calculations is that the image calculation is purely numerical, and although very convenient to generate actual images, the overall effect can be assessed more readily by making use of the pseudo-weak-phase-object approximation (PWPOA; Li and Tang 1985), which obtains an analytical expression for the scattering as a function of depth in the crystal if each slice can be treated as a weak phase object and terms involving $\varphi^2(x, y)$ are ignored. In this approximation, the wavefunction after the $(n + 1)$th slice at the optimum defocus is given by

$$\psi_{n+1}(x, y) = 1 - \sigma\varphi(x, y) - \sigma\varphi(x, y) * \sum_{j=1}^{j=n} S_j(x, y) - i\sigma\varphi(x, y) * \sum_{j=1}^{j=n} C_j(x, y)$$

where $*$ represents the operation of convolution and S_j and C_j are Fresnel sine and cosine functions of order j defined thus:

$$S_j = (1/j\lambda\Delta z)\sin(\pi/j\lambda\Delta z)(x^2 + y^2) \qquad C_j = (1/j\lambda\Delta z)\cos(\pi/j\lambda\Delta z)(x^2 + y^2).$$

In effect, therefore, the PWPOA attributes the overall changes in the wavefunction as a function of depth in the crystal as arising solely from the propogation terms, which are expressed in the Fresnel sine and cosine functions. If absorption is considered, we merely replace σ by $\sigma - i\gamma$ above, and the resulting image *intensity* after the $(n + 1)$th slice at the optimum defocus becomes

$$\begin{aligned} I_{n+1}(x, y) = 1 &- 2\sigma\varphi(x, y) + (\sigma^2 + \gamma^2)\varphi^2(x, y) - 2\sigma\varphi(x, y) * \Sigma S_j(x, y) \\ &- 2\gamma\varphi(x, y) * \Sigma C_j(x, y) + 2\sigma^2\varphi(x, y)(\varphi(x, y) * \Sigma S_j(x, y)) \\ &+ (\sigma^2 + \gamma^2)(\varphi(x, y) * \Sigma S_j(x, y)) + (\sigma^2 + \gamma^2)(\varphi(x, y) * \Sigma C_j(x, y)) \end{aligned}$$

which, if I_0 is taken as the wave intensity when absorption is neglected, can be simplified to

$$\begin{aligned} I_{n+1}(x, y) = I_0 &- 2\gamma\varphi(x, y) * \Sigma C_j(x, y) + \gamma^2[\varphi^2(x, y) + (\varphi(x, y) * \Sigma S_j(x, y))^2 \\ &+ (\varphi(x, y) * \Sigma C_j(x, y))^2]. \end{aligned}$$

As γ is generally small, we can then neglect all terms except the first two, obtaining

$$I_{n+1}(x, y) = I_0 - 2\gamma\varphi(x, y) * \Sigma C_j(x, y).$$

The effect of absorption can then be seen to be a reduction of the overall contrast, as expected, but because the absorption term includes the convolution with the summation of the Fresnel cosine functions, the effect will be greatest at the positions of high potential density, namely at the centres of heavy atoms, and, as the number of slices and consequently the maximum value of j increases, the influence of this summation on the intensity will also become greater. Consequently as the thickness increases, the contrast at light atoms will tend to increase relative to that of heavy atoms, making them more readily visible, as has already been demonstrated in the case of lithium atoms (Tang *et al* 1986, 1989). In the above discussion, it has been assumed that γ is the same for all atoms: if this is not so, we must replace γ by $\gamma(x, y)$ and the effect will be the same, except that it will be greater at atoms where γ is higher.

The simulations in figure 1 show the general effect on images of $YBa_2Cu_3O_{7-x}$ in both [100] and [010] projections at constant specimen thickness, in this case 8.0 nm, and at the optimum focus when the value of the absorption coefficient is increased. All these

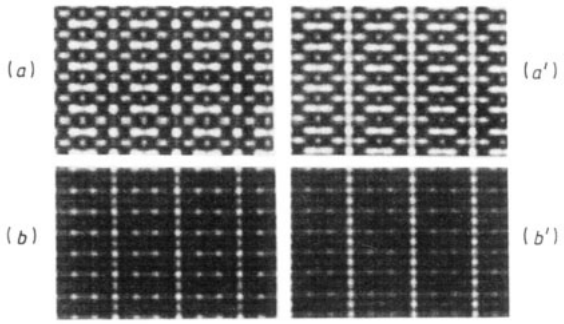

Figure 2. Image simulations with varying contrast scales to indicate the slight alterations in contrast pattern. (*a*) and (*a'*) are identical to (*a*) and (*a'*) in figure 1, and (*b*) and (*b'*) are the same as (*d*) and (*d'*) in figure 1 but with the contrast stretched.

images are on the same absolute contrast scale, and the overall pattern of the diminution of contrast can be clearly observed. In figure 2, however, the first pair of images ((*a*) and (*a'*)) are identical to those of figure 1, while the second pair ((*b*) and (*b'*)) are the same as the last pair in figure 1, but with the contrast scale artificially enhanced to bring out the detail, when differences in the actual pattern of contrast become noticeable. For example, in the first pair of images all the atoms except oxygen appear as white dots and the channels between the two square-planar coordinated copper atoms, seen in the [010] projection of figure 2(*b'*), also appear white. In the second pair, however, the contrast at the yttrium and barium atoms has become dark, while that at the copper positions is almost unchanged, and the oxygen atom between the square-planar coordinated copper atoms in figure 2(*b*) is almost as bright as the channel in the equivalent position in figure 2(*b'*). This behaviour is that predicted by the PWPOA theory, and clearly illustrates the dangers of assuming that white dots can be taken as representing structural channels, even in relatively thin crystals, if absorption occurs. For other defocus values, the effects observed in simulations are equally strong, although the PWPOA expression becomes much more complex when an aberration function must also be included, and cannot therefore be interpreted so readily.

3.2. Elastic scattering of initially inelastic electrons

The principal differences between the *elastic* image and those formed by the elastic scattering of initially *inelastic* electrons will lie in the fact that, because the latter are of slightly longer wavelength, the optimum defocus position will be different for the latter and the modification of the image contrast by the phase contrast transfer function will also differ. The final image can be regarded as the sum of several different images, the main one being the elastic image corresponding to the no-loss peak in the EELS, with other inelastic images being equivalent to the various plasmon- and core-loss peaks in the EELS spectrum. For all the images, their particular focal spread will be determined by the width of the appropriate peak, and the magnitude of their contribution to the overall image is governed by their relative peak area in the EELS spectrum. Consequently, if the specimen is thick, or if the inelastic processes are strong, the combined sum of the inelastic images with their different contrast patterns may well swamp the contrast of the elastic image. However, their effect will be reduced if the plasmon peaks are relatively broad; as a consequence of the resulting large focal spread there will be a diminution of

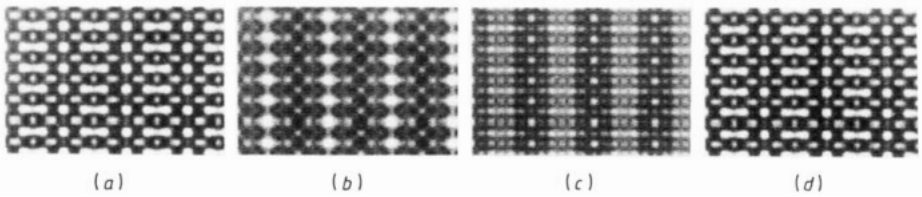

Figure 3. [100] simulated images for 8.0 nm thickness showing the differences between elastic and inelastic components of the image. (*a*) The elastic component. (*b*), (*c*) Components formed by the peaks II and III in table 1. The numbers of sampling points used for the focal spread calculation were 15, 43 and 95 respectively. (*d*) The overall image, with the three components combined with the weights of table 1.

the contrast of that particular image component, and, in the limit where the EELS spectrum is just broad and featureless, the net effect will be exactly the same as adding an approximately constant background intensity. For any assessment of possible contributions from these inelastic image comonents, therefore, an examination of the EELS spectrum of the specimen *at a known specimen thickness* will be necessary.

Table 1 shows the results of an analysis of a deconvoluted EELS spectrum of a relatively thin crystal of $YBa_2Cu_3O_{7-x}$ in terms of measured weighting, effective relative defocus and focal spreads. The latter were calculated, after separation of the complex low-loss peak into two overlapping peaks, according to the expression

$$\Delta f = Cc\Delta V/V_0.$$

From spectra such as this determined at different thicknesses, an estimation of the variation of the relative weighting with thickness could be made, and then applied to images calculated at other thickness values. Of the many peaks in the EELS spectrum, only the two overlapping plasmon peaks corresponding to relatively small energy losses were of sufficient magnitude to contribute in any way to the image. All of the others detected, such as the oxygen K, copper $M_{2,3}$ and $L_{2,3}$, and yttrium $N_{2,3}$ and $M_{4,5}$ edges (the former being just visible at the edge of the composite plasmon-loss peak in figure 1), and the barium $M_{4,5}$ and $N_{4,5}$ edges were either of negligible area or so broad that the focal spread of the images so generated would have been enormous. For the loss peaks used, the effect of V on the scattering interaction parameter σ was ignored as the value of V/V_0 was less than 10^{-4}. A trial simulation which actually used the slightly different values of the electron wavelength in the multi-slice procedure was compared with one where the same wavelength was used for all the component images and their relative focal positions altered accordingly, and, at the specimen thicknesses used, the differences were so slight that the latter method, being much the simpler to apply, was used for all subsequent calculations.

Figure 3 shows how dramatically the contrast in the component images varies at even the small energy-loss values used. The pattern of contrast of the elastic image (figure 3(*a*)) differs completely from that corresponding to images from the two loss peaks considered (II and III respectively) which are shown in figures 3(*b*) and (*c*). When the relative weights are considered and the images summed, however, as shown in figure 3(*d*), where the weights are those of table 1 and the specimen is 8 nm thick, the preponderance of the elastic image is clearly demonstrated, and the overall contrast pattern is little different from that obtained by neglecting the inelastic components completely. Even if the magnitude of the inelastic scattering is artificially enhanced, as shown in

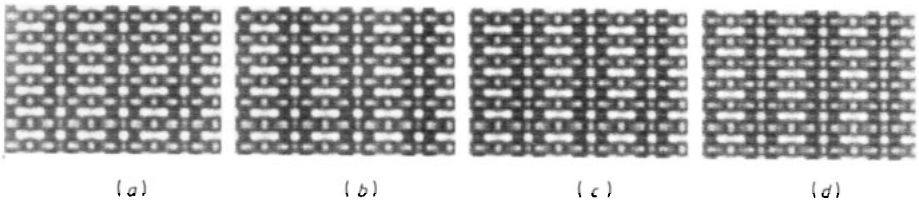

Figure 4. Images simulated with the same conditions as for figure 3(*d*) but with the weight of the elastic component decreased to 0.7, 0.6, 0.5 and 0.4 respectively.

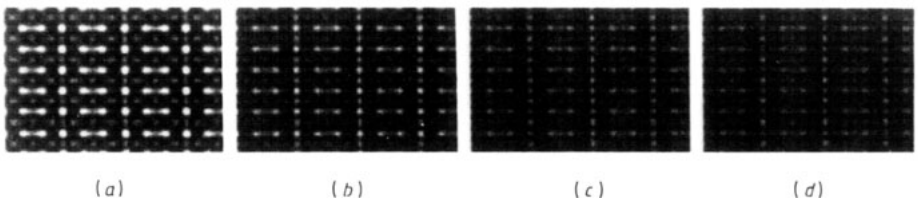

Figure 5. [100] simulations showing the effect of absorption and inelastic scattering combined. The values of the absorption coefficient and component relative weights are: (*a*) $y = 0.0001$, weights 0.767, 0.030, 0.203; (*b*) $y = 0.0003$, weights 0.569, 0.056, 0.375; (*c*) $y = 0.0005$, weights 0.457, 0.070, 0.472; (*d*) $y = 0.0007$, weights 0.380, 0.081, 0.539.

figure 4 where the weight of the elastic component of the image is reduced from 0.7 to 0.4 (as compared with 0.831 for figure 3), the overall pattern of contrast does not change dramatically, although the overall magnitude of the contrast is reduced. Some changes however, are evident if the simulation with maximal inelastic contribution (figure 4(*d*)) is compared with a purely elastic image (figure 3(*a*)). Then it can be seen that the effect of including the inelastic image components is to decrease greatly the overall contrast of the copper atoms adjacent to the plane of yttrium atoms: these are arrowed in figure 4(*d*). Apart from a preferential removal of contrast at these planes, however, the overall pattern of the image detail remains the same, and we must therefore conclude that for a specimen thickness of 8 nm, typical of the value used for previous HREM studies (Zhou *et al* 1987), the effect of inelastic components on the image contrast is not generally significant.

3.3. Absorption and inelastic scattering combined

A series of images was calculated for the same specimen thickness (8 nm) but including the effects of both absorption and inelastic components of the image is shown in figure 5, the latter being combined with the same relative weights as before. These images differ from those of figure 4 only in as much as the elastic component of the total image in this case includes the amplitude contrast term. No allowance was made for amplitude contrast in the inelastic components, therefore ruling out the possibility of repeated inelastic scattering. For the specimen thickness used, this was valid as the actual absorption edges present in the EELS were relatively sharp. In thicker specimens, however, a loss of sharpness in these edges has been attributed to repeated inelastic events and these would have to be included, although the computational problems are then considerable. It was also assumed in the calculations that the relative weights of the inelastic components did not change with specimen thickness.

The calculations for the combined absorption/inelastic images were also performed in two ways as referred to above, one using the same set of diffracted beams for the specimen thickness for all the image components, these components then differing only because their effective defocus positions were different, and the second method using the different wavelengths in both the multiple-scattering and image calculations. As the differences were minimal, the former approach was used throughout. Tests were also made to ascertain whether it was necessary to increase the total scattering in the inelastic images progressively, using a negative absorption coefficient, corresponding to electrons being diverted from the elastic to the inelastic image components, as actually occurs in the specimen, or whether the inelastic component could be calculated at a constant total weight and then multiplied by the appropriate weighting factor at the end of the calculation. Again the differences were minimal, and the latter method was used because of its simplicity.

In figure 5(*a*) with the bulk absorption coefficient set at 0.0001, the general pattern and level of contrast in the image is much the same as in figure 1(*b*), indicating that amplitude scattering in the elastic image is the principal reason for the changes in contrast, despite the fact that a lesser weight is given to this image than in the actual specimen of this thickness (0.767 compared to 0.831). In figures 5(*b*) and 5(*c*), where the absorption coefficient increases from 0.0003 to 0.0007, the alteration of the overall contrast is almost identical to that of figures 1(*c*) and 1(*d*), showing that even in the presence of strong inelastic components in the image, the effect of amplitude contrast in the elastic image remains the most dominant influence. Even in figure 5(*d*), where one of the inelastic components has a weight exceeding 50%, the changes in the pattern of contrast described in the preceeding section are almost imperceptible compared with those arising from amplitude scattering.

4. Conclusions

The overall conclusions of the study described here are that, for a specimen thickness of 8 nm, a value typical of that used for the recording of HREM images of crushed specimen fragments, the overall pattern of image contrast is not significantly affected by either amplitude contrast or by images formed from inelastically scattered electrons, and that of the two effects, amplitude scattering is the more important. It should, however, be stressed that this value of specimen thickness is near the lower end of the range of thicknesses normally encountered, and that many images of defect structures, in particular, come from considerably thicker specimens. Then, as can be seen from the effect of artificially enhanced absorption described above, the overall magnitude of contrast may be significantly altered to such an extent that structural detail is difficult to discern. Furthermore, for thicker specimens the use of an overall bulk absorption coefficient may not be valid, and data must then be determined to assign imaginary components to the structure factors of individual atoms. For thicker specimens also, repeated inelastic events will have to be considered, giving rise to an ever more complex pattern of components in the image. Before any interpretation can be made in these cases therefore, some assessment of the magnitude and type of the inelastic processes occurring must be made, by obtaining EELS data from the actual area of interest or, alternatively, the inelastic components must be removed by energy filtering.

Acknowledgments

DT wishes to acknowledge the Royal Society for the award of a Queen Elizabeth Fellowship. We are grateful to the SERC for general support and for a research studentship for RDB.

References

Allpress J G, Hewatt E A, Moodie A F and Sanders J V 1972 *Acta Crystallogr.* A **28** 528–36
Boothroyd C B and Stobbs M W 1987 *Electron Microscopy and Analysis 1987* (Inst. Phys. Conf. Ser. 90) pp 237–40
Cowley J M 1979 *Chem. Scr.* **14** 279–85
Cowley J M and Moodie A F 1957 *Acta Crystallogr.* **10** 609–19
Crowther R A and Klug A 1975 *Ann. Rev. Biochem.* **44** 161–80
Ekstrom T and Tilley R J D 1978 *J. Solid State Chem.* **24** 209–18
Goodman P and Moodie A F 1974 *Acta Crystallogr.* A **30** 280–90
Grinton G R and Cowley J M 1971 *Optik* **34** 221–30
Grzinic G, Bursill L A and Smith D J 1983 *J. Solid State Chem.* **47** 151–63
Hanzen K J 1971 *Adv. Opt. Electron Microsc.* **4** 1–21
Hashimoto H 1985 *Ultramicroscopy* **18** 19–32
Iijima S and Allpress J G 1974 *Acta Crystallogr.* A **30** 22–9
Jefferson D A, Uppal M K, Rao C N R and Smith D J 1984 *Mater. Res. Bull.* **19** 1403–9
Lanio S, Rose H and Krahl D 1986 *Optik* **73** 56–68
Li F H and Tang D 1985 *Acta Crystallogr.* A **41** 376–82
Stobbs M W and Saxton W O 1989 *J. Microsc.* at press
Tang D, Jefferson D A, Pickering I J, Harriman A, Thomas J M and Brydson R D 1989 *J. Solid State Chem.* at press
Tang D, Teng C M, Zou J and Li F H 1986 *Acta Crystallogr.* B **42** 340–2
Williams B G, Egerton R F and Sparrow T G 1985 *Proc. R. Soc.* A **398** 395–404
Yuan J, Brown L M and Liang W Y 1988 *J. Phys. C: Solid State Phys.* **21** 517–26
Zhou W, Jefferson D A and Thomas J M 1986 *Proc. R. Soc.* A **406** 173–82
Zhou W, Thomas J M, Jefferson D A, Mackay K D, Shen T H, Van Damme I and Liang W Y 1987 *J. Phys. F: Met. Phys.* **17** 173–7